Selection of Low Dimensional Material Alternatives to Silicon for Next Generation Tunnel Field Effect Transistors

Pratyush Manocha[1] · Kavindra Kandpal[3] · Rupam Goswami[2]

Abstract

This paper presents a method-based investigation on the application of low dimensional materials like graphene, carbon nanotube (CNT), transition metal dichalcogenides (TMDCs) in tunnel field effect transistors (TFETs) for high on-current requirements. Three multi-criteria decision making methods (MCDM) are employed to arrive at a consensus on the appropriate material. The Ashby technique, the Technique for Order Preference by Similarity to Ideal Solution (TOPSIS) and VlseKriterijumska Optimazicija I Kompromisno Resenjein in Serbian (VIKOR) are utilized using constraints which decide a TFET's performance. In order to select the material, dominant parameters have been included in the formulation which includes intrinsic material properties like the band gap, dielectric constant and electron effective mass along with an extrinsic parameter, namely, the on-state current to the off-state current ratio. The analysis demonstrates a remarkable agreement between the results of Ashby, TOPSIS and VIKOR methods, and concludes that carbon nanotube (CNT) has the most potential amongst all the candidates to be employed in the next generation TFETs.

Keywords Ashby · TOPSIS · VIKOR · TFET · 2D materials · Carbon nanotube · Silicon

1 Introduction

The use of complementary metal-oxide-semiconductor (CMOS) technology has been on the rise since the last three decades and has today established itself as the preferred topology for many circuit design engineers worldwide [1]. The CMOS technology permits scaling of metal-oxide-semiconductor field effect transistors (MOSFETs) to achieve a faster performance and results in a good performance-to-cost ratio. However, continuing this rigorous scaling into the nanometre regime leads to a severe degradation in performance due to problems like short channel effects (SCE), high field velocity saturation affecting the on-state current (I_{on}), and an increase

✉ Rupam Goswami
   rup.gos@gmail.com

1   Department of Electrical and Electronics Engineering, Birla Institute of Technology and Science, Pilani, Rajasthan, India

2   Department of Electronics and Communication Engineering, Tezpur University, Napaam, Assam, India

3   Department of Electronics and Communication Engineering, Indian Institute of Information Technology Allahabad, Pragyaraj, Uttar Pradesh, India

in the influence of parasitic resistances and capacitances on the on-state current (I_{on}) [1, 2]. The most critical out of the above mentioned problems is the short channel effect, caused by a decrease in the spacing between the source (S) and drain (D) junctions. This leads to two phenomena, namely, drain induced barrier lowering (DIBL) and threshold voltage roll-off (V_t roll-off) [1, 3] which have been explored in depth and explained very well in standard texts [4, 5].

In an attempt to combat this degradation in the device performance, various designs had been proposed and have since been adopted in use. One such design is the tunnelling field effect transistor (TFET) which works on the principle of band to band tunnelling (BTBT) [6]. The structure of a TFET is similar to a MOSFET and contains a source and a drain junction. The only difference is that a TFET may contain multiple gates and is a multi-gate (MuG) device. Unlike a MOSFET where the current is generated through thermionic emission, the current in a TFET comes from the quantum mechanical tunnelling of the minority carriers from the source to the channel. The applied gate voltage serves to modulate the barrier height between the source and the channel and facilitates the achievement of low off-state current (I_{off}) due to less tunnelling probability in the off-state. This device design has reported large values of on-state current to the off-state current ratio

(I_{on}/I_{off}), exceptional subthreshold behaviour with sub-KT/q values of the subthreshold swing (SS) and less SCEs [6–8]. While this device demonstrates a remarkable operation on all fronts, it faces certain shortcomings like the ambipolar nature of I_{on} and low I_{on} value. Ambipolarity prevents the device from turning off and contributes to leakage current in the device. This problem can be reduced by modifying the structure to include either or all of the strategies in [9]: non-uniform doping in the source and drain junctions [10, 11], gate-drain underlap [12], gate-drain overlap [13, 14] and dual gate dielectric materials [15].

The low value of I_{on}, however, cannot be tackled by simple modifications to the general structure and is a major concern for the device engineers all across the globe. To overcome this hurdle, various structures like the dual source TFET (DS-TFET) [16], Double gate TFETs [10], nanowire TFETs [17], gate all around TFETs [18, 19], dual-metal-gate TFETs [20], gate-on-source only TFET [21], gate-on-source/channel TFET [22], L-shaped TFET [23], heterojunction TFETs [24, 25], Carbon nanotube TFETs [26], 2D material TFETS [27] and Van der Waals Heterostructure TFETS [28] have been proposed.

Amongst all the aforementioned architectures, the least explored, by far, are the 2D material TFETs. Two dimensional materials, or 2D materials in short, are materials with one direction of electron transport quantised (in nano-scale dimensions). These nano-sheet materials like graphene, transition metal dichalcogenides (TMDCs), phosphorene, hexagonal boron nitride (h-BN) and xenes have exceptional electrical, mechanical and magnetic properties. These materials have especially high carrier mobilities, lower band gap and lower dielectric constant, which when used in a TFET, can result in a higher on-current and a reduced DIBL effect. As was discussed above, the performance of a TFET is heavily dependent on the amount of current it can provide and the steepness of subthreshold slope that it can afford and the application of these materials can effectively boost the performance of the device. Despite the patent advantages that these materials offer, they have challenges of their own and have to be used carefully. To begin with, the nano-sheets are difficult to synthesize and care must be taken in their handling because they are fragile and can be ruptured or damaged very easily. In addition to this, these materials do not have an established method to precisely control the fermi level [29], a factor that is essential for electronic applications. It is also true that since these novel materials have recently been developed, there isn't much research conducted on them. Therefore, it's of primary importance to evaluate the different electrical parameters arising out of the application of these 2D materials as channel materials in the tunnelling transistors through a systematic and scientific approach. Many such approaches have been proposed over time, oriented towards appropriate material selection strategies. Such approaches have already been applied for material selection in MOSFETs [30], TFETs, other transistors [31] and the engineering regime [32], in general. These methods assist a device engineer to arrive at concrete conclusions based on quantitative analyses and weight-based rankings.

As there are various low dimensional materials used as channels in TFETs in the literature, with each material having its own set of benefits and limitations, one can employ a multi-criteria decision making (MCDM) approach to deduce the ideal choice of the material. The MCDM method is broadly classified into two categories, the multi-objective decision making (MODM) and the multi-attribute decision making (MADM) methods. The Ashby method [33, 34] under MODM and the TOPSIS and VIKOR methods [35, 36] under MADM are some of the eminent approaches and are drawn upon in this work.

This paper is organised as follows: Section 2 deals with a TFET and its determining properties. Section 3 is a discussion of the material selection approaches adopted by this work. Section 4 discusses the material indices and goes over the construction of the fundamental decision matrix. Section 5 presents the results of the study and Section 6 states the conclusions drawn by the work.

2 TFETs and their properties

Figure 1 shows a schematic view of a low dimensional material TFET in which a low dimensional material acts as a channel between the drain and the source junctions of the TFET. The 2D films are usually obtained by exfoliation or grown by CVD on a suitable substrate. These films are then transferred onto the desired substrate (device) using a mechanical transfer method [37, 38]. This implies that the channel material in the device is prone to defects and care should be taken to ensure that it's pristine and free of defects of any kind to obtain high performance.

Since a TFET works on quantum mechanical tunnelling, the current in the device is of a probabilistic nature and is directly proportional to the tunnelling probability of the minority carrier from the source to the channel through the source-channel barrier. According to the Wentzel Kramers Brillouin (WKB) approximation the Tunnelling probability [8] is:
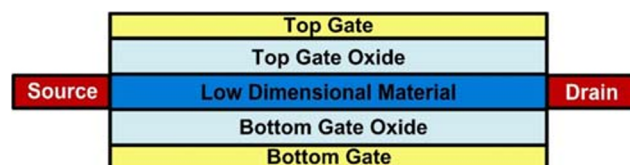

Fig. 1 Schematic of a Low Dimensional Material TFET

$$T_{wkb} \approx e^{\frac{-4w\sqrt{2m_e^* E_g^3}}{3qh[E_g + \Delta\Phi]}} \tag{1}$$

where E_g is the bandgap of the material, m_e^* is the effective mass of electrons (in conduction band), $\Delta\Phi$ is the overlap between VB and CB at the source & drain junctions, and w is the tunnel width which is given by:

$$w = \sqrt{\frac{\varepsilon_{ch}}{\varepsilon_{ox}} t_{ch} t_{ox}} \tag{2}$$

where ε_{ch}, ε_{ox} are the dielectric constants of the material and the oxide respectively, while t_{ch}, t_{ox} are the thicknesses of the material and the oxide respectively.

From the above eqs. (1) and (2), it's clear that for high on-current, the material needs to have low effective mass of electrons (in conduction band), low bandgap and low tunnelling width which can be extrapolated to low dielectric constant for materials with the same layer thickness.

An important factor to consider for the scalability and the SCE in the device is the natural scaling length λ. The natural scaling length in double gated FETs [39] is defined as:

$$\lambda = \sqrt{\frac{\varepsilon_{ch}}{2\varepsilon_{ox}} \left(1 + \frac{\varepsilon_{ox} \, t_{ch}}{4\varepsilon_{ch} \, t_{ox}}\right) t_{ch} t_{ox}} \tag{3}$$

which can also be written as,

$$\lambda = \sqrt{\left(\frac{\varepsilon_{ch}}{2\varepsilon_{ox}} + \frac{1}{8}\frac{t_{ch}}{t_{ox}}\right) t_{ch} t_{ox}} \tag{4}$$

A lower value of λ helps in reducing the SCEs, making the device behaviour similar to that of a long channel transistor and ultimately resulting in a more scalable device. Therefore, it can be said that the dielectric constant of the channel has to be low to allow for the device to be robust and scalable.

According to the above discussions, the ideal material to employ in a TFET channel is one with a low bandgap, low dielectric constant, and a low effective mass of electrons (in conduction band). The low bandgap leads to a smaller barrier for tunnelling and increases the I_{on}, which is a desirable property, however, having an extremely low bandgap will contribute to off-state leakage currents in the device and will lead to degradation of the I_{on}/I_{off} ratio. This makes it imperative to consider experimental data and use the I_{on}/I_{off} ratio as an attribute for the selection of the best possible alternative.

3 Material Selection Approaches

Ashby [33, 34] is one of the most prevalent multi-objective decision making approaches because it selects the best material based upon priorities and limits on acceptable ranges of the objectives. On the other hand, TOPSIS [35] and VIKOR [36], the multi-attribute decision making methods, are widely used and preferred because they shortlist the best alternative(s) based upon a weighted ranking system of the attributes. Ashby analysis is qualitative and requires the use of a 'figure of merit function' to isolate the ideal choice. In contrast to this, TOPSIS and VIKOR are quantitative in nature and assign ranks to the various substitutes available. TOPSIS method is based on the concept that the chosen alternative has the minimum possible distance from the positive ideal solution and the maximum possible distance from the negative ideal solution, while VIKOR determines the compromised solution by deriving least individual regret of the opponent and the maximum group utility of majority.

Depicted in Fig. 2 is a flow chart illustrating the various steps used in figuring out the best channel material for a TFET device. The first step involves finding all the materials that have been used as TFET substrates. M. Strojnik $et.\ al$ have fabricated MoS_2 nanotube FET using a two-step synthesis method [40]. Joerg Appenzeller $et.\ al$ have shown a TFET with CNT as the substrate [41]. Similarly, the materials depicted in this paper have been successfully demonstrated by various researchers to be studied for their use in a device [27, 39, 42]. The next step is noting down material indices like band gap, out-of-plane dielectric constant, electron effective mass of conductivity and on-state current to off-state current ratio to construct the fundamental decision matrix. This is followed by the application of the material selection methodologies and the comparison of the results.

3.1 Ashby Approach

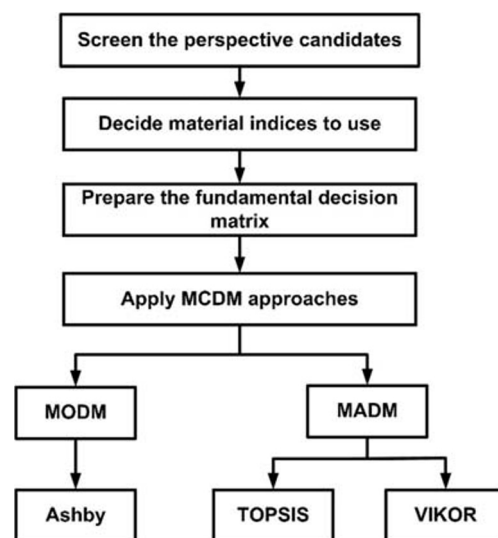The Ashby approach involves mainly four steps, which are

Fig. 2 Flow chart of material selection approach

1. Translating objectives and constraints into design requirements
2. Screening using various constraints
3. Finding out suitable set of solution using objectives
4. Validating results with experimental data, if available.

The objective is to maximise the on-current of the device. This is translated into the following constraints:

1. Band-gap should be low (< 1.1 eV)
2. Dielectric constant should be low (< 5)
3. Effective mass of electrons should be low (<0.4m_0), where m_0 is the rest mast of a free electron

The variables for the analysis are the choice of materials and the material indices (M) are band gap (E_g), out-of-plane dielectric constant (ε_r) and the effective mass of electrons (in conduction band) (m_e^*). To define the Ashby function of device performance P, a functional parameter (F) and a geometrical parameter (G) needs to be defined. The functional parameter is chosen to be the on-current in the device (I_{on}) while there is no geometrical parameter defined. Therefore, P can be written as: $P = f(F, M)$.

To quantify the results, an appropriate figure of merit (FOM) is to selected. The figure of merit chosen is closely linked to the device performance P and is given by:

$$\text{FOM} = \frac{\sqrt{\frac{11.7}{\varepsilon_{ch}} \ln\left(\frac{I_{on}}{I_{off}}\right)}}{E_g^2 m_e^*} \qquad (5)$$

The FOM has been formulated in a manner so that it consists of the significant parameters required to assess the performance of a 2D material based TFET. Higher the value, better is the device. It is evident from Section 2 that the tunnelling probability, and hence the drain current in a TFET is inversely related to the energy bandgap of the material constituting the tunnelling area. A low bandgap is always preferred for a high tunnelling rate. However, it must also be noted that a low bandgap encourages high off current as well. For a TFET to operate in low power, its leakage current is an essential parameter. Hence, a high ratio of on and off currents (I_{on}/I_{off}) along with high on current indicates a device with reasonably low off current. Since the value of this ratio is usually expressed in an exponent of 10, so a logarithmic expression is used to suppress the numerical dominance of the parameter over others. A low material dielectric constant is preferred for a low scaling length as expressed in (4). Therefore, it has been considered as a dependent parameter in the expression for FOM. This parameter is expressed as a ratio with respect to the dielectric constant of Silicon as it can possess higher values. The electron effective mass is another inversely related

quantity which decides high channel mobility, and has been taken as a parameter in the FOM.

3.2 TOPSIS Approach

This approach, which was developed by Ching-Lai Hwang and Yoon in 1981 [35], is based on the concept of closeness of the best alternative to the ideal choice by minimising the distance from the positive ideal solution (PIS) and maximising the distance from the negative ideal solution (NIS). The PIS is the solution that maximises the profit criteria while minimising the cost criteria whereas NIS is the solution that minimises the profit criteria and maximises the cost criteria. This method is one of the most widely used procedures [43–45] and is very versatile as is shown by the fact that it can very easily be clubbed with type-2 fuzzy sets to give interval type-2 fuzzy TOPSIS method, as was shown by Liao [44]. In addition to being prevalent in material selection problems, this method is considered veritable and is used to verify the results of other MODM and MADM criteria. There are six steps in this method, which are as follows:

Step 1. The decision matrix is normalised.

The decision matrix elements r_{ij} are normalised by dividing by the RMS value of each attribute.

$$p_{ij} = \frac{r_{ij}}{\sum\limits_{i=1}^{m} (r_{ij})^2} \qquad (6)$$

where i is the index of the set of m materials and j is the index of the set of n attributes.

Step 2. The weighted normalised matrix is computed.

$$t_{ij} = w_j * p_{ij} \qquad (7)$$

where w_{ij} is the weight assigned to the n attributes such that $\sum\limits_{j=1}^{n} w_j = 1$.

Step 3. PIS and NIS are computed.

The positive ideal solution, PIS is defined as: PIS = S^+ = $\{t_1^*, t_2^*, \ldots, t_n^*\}$ = $\{\max(t_{ij}) | j \in A^+\}$ or $\{\min(t_{ij}) | j \in A^-\}$

The negative ideal solution, NIS is defined as: NIS = S^- = $\{t_1^-, t_2^-, \ldots, t_n^-\}$ = $\{\min(t_{ij}) | j \in A^+\}$ or $\{\max(t_{ij}) | j \in A^-\}$, where A^+ is the profit criteria and A^- is the cost criteria.

Step 4. Euclidean distances from PIS and NIS are calculated.

Distance from PIS:

$$Q_i^* = \sqrt{\sum_{j=1}^{n} \left(t_{ij} - t_j^*\right)^2} \, \forall i = 1, 2, \ldots, m \qquad (8)$$

Distance from NIS:

$$Q_i^- = \sqrt{\sum_{j=1}^{n} \left(t_{ij} - t_j^-\right)^2} \, \forall i = 1, 2, \ldots, m \qquad (9)$$

Step 5. The relative closeness to ideal solution is calculated.

The relative closeness, RC* is defined as

$$\text{RC}^* = \frac{Q_i^-}{Q_i^- + Q_i^*} \, \forall i = 1, 2, \ldots, m \qquad (10)$$

Step 6. Ranks are allotted to all materials

The alternatives are allotted a rank based on the descending order of the RC* value (closeness to 1). The higher the RC* value, the better is the performance of the material.

3.3 VIKOR Approach

The VIKOR approach, originally developed by Serafim Opricovic [46] is a MADM approach that solves decision problems with conflicting and non-commensurable (different units) criteria by offering a set of alternatives as a compromise solution in the capacity of the criteria in question. There are six steps in this method, which are as follows.

Step 1. Maximum and minimum values are determined.

For decision matrix element r_{ij} with i as the index of the set of m materials and j as the index of the set of n attributes, the maximum (r_j^*) and the minimum $\left(r_j^-\right)$ values are:

$$r_j^* = \left\{ \max\left(r_{ij}\right) \mid j \in A^+ \right\} \text{ or } \left\{ \min\left(r_{ij}\right) \mid j \in A^- \right\} \forall i$$
$$= 1, 2, \ldots, m$$

$$r_j^- = \left\{ \min\left(r_{ij}\right) \mid j \in A^+ \right\} \text{ or } \left\{ \max\left(r_{ij}\right) \mid j \in A^- \right\} \forall i$$
$$= 1, 2, \ldots, m$$

where A^+ is the profit criteria and A^- is the cost criteria.

Step 2. The maximum group utility (GU) and the minimum individual regret (IR) are calculated.

$$\text{GU}_i = \sum_{j=1}^{n} w_j * \left(\frac{r_j^* - r_{ij}}{r_j^* - r_j^-} \right) \qquad (11)$$

$$\text{IR}_i = \max_j \left[w_j * \left(\frac{r_j^* - r_{ij}}{r_j^* - r_j^-} \right) \right] \qquad (12)$$

where w_j is the weight assigned to the n attributes such that $\sum_{j=1}^{n} w_j = 1$

Step 3. The maximum and minimum values for GU and IR are calculated.

The maximum (GU$^-$) and minimum values (GU*) for GU are given by

$$\text{GU}^- = \max(\text{GU}_i)$$

$$\text{GU}^* = \min(\text{GU}_i)$$
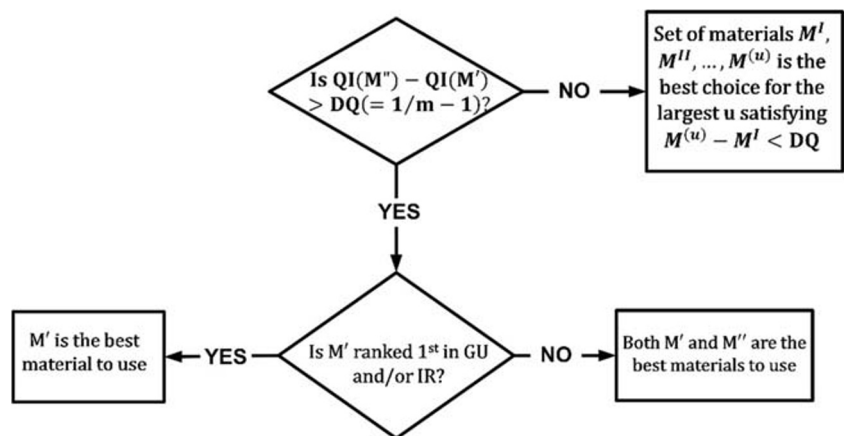
Fig. 3 VIKOR decision criteria

Table 1 Electron effective mass of conductivity of Si, Ge

Material	Effective electron mass (longitudinal) m_l^*	Effective electron mass (transverse) m_t^*	Effective electron mass of conductivity m_{cc}^*
Si	$0.91m_0$	$0.19m_0$	$0.26m_0$
Ge	$1.59m_0$	$0.0815m_0$	$0.12m_0$

The maximum (IR^-) and minimum values (IR^*) for IR are given by

$$IR^- = \max(IR_i)$$

$$IR^* = \min(IR_i)$$

Step 4. The quality index (QI) is computed.

$$QI_i = \mu\left(\frac{GU_i - GU^*}{GU^- - GU^*}\right) + (1 - \mu)\left(\frac{IR_i - IR^*}{IR^- - IR^*}\right) \qquad (13)$$

where μ is the weight of strategy GU_i and $(1 - \mu)$ is the weight of strategy IR_i.

According to the value of μ, the decision making process is divided into three types.

1. If $\mu > 0.5$, the decision making process is called "voting by majority rule".
2. If $\mu = 0.5$, the decision making process is called "voting by consensus".
3. If $\mu < 0.5$, the decision making process is called "voting by veto".

Amongst the three types of decision making processes, the most common is "voting by consensus" and is applied in this work.

Step 5. Ranks are allotted based upon GU, IR and QI.

Ranks are allotted to materials in the alternative set according to the ascending order of the data in GU, IR and QI respectively. The materials are labelled M', M'', …, $M^{(m)}$ according to their rank in QI.

Step 6. The best alternative is proposed based on the following conditions.

The decision quotient, $DQ = \frac{1}{m-1}$ where m is the number of materials in the alternative set.

Conditions:

C1. Acceptable advantage

$$QI\left(M''\right) - QI\left(M'\right) \geq DQ \qquad (14)$$

C2. Acceptable stability in decision making

Material $\acute{M}$ is the best ranked in either or both of ranking series generated using GU and IR.

Therefore, material $\acute{M}$ is the best alternative.

However, if any of the above conditions is violated, a set of compromise solutions is proposed as follows.

CS1. Only condition of acceptable advantage is violated.

Materials M', M'', …, $M^{(u)}$ are best materials as is required by the modified decision criteria which is given by:

$QI(M^{(u)}) - QI(\acute{M}) < DQ$ for the maximum possible u. (15)

CS2. Only condition of acceptable stability in decision making is violated

Materials M' and M'' are the best alternatives.

Figure 3 depicts a flow chart to visually express the decision making conditions.

Table 2 Fundamental decision matrix

Material	E_g	m_e^*	ε_r	$\frac{I_{on}}{I_{off}}$
MoS$_2$	1.6800	$0.52m_0$	2.8000	3.0000×10^2
MoTe$_2$	1.0800	$0.57m_0$	4.4000	2.3000×10^3
WSe$_2$	1.5600	$0.36m_0$	2.9000	4.6000×10^3
WTe$_2$	0.7500	$0.37m_0$	3.3000	1.2700×10^5
Graphene (bilayer)	0.0500	$0.037m_0$	6.9000	1.0000×10^1
CNT	0.7000	$0.1m_0$	1.0000	1.0000×10^3
Si$_{0.73}$Ge$_{0.27}$	1.0099	$0.26m_0$	13.020	1.0000×10^7
Si	1.1200	$0.26m_0$	11.700	1.0000×10^8
Ge	0.6610	$0.12m_0$	16.200	1.0000×10^3
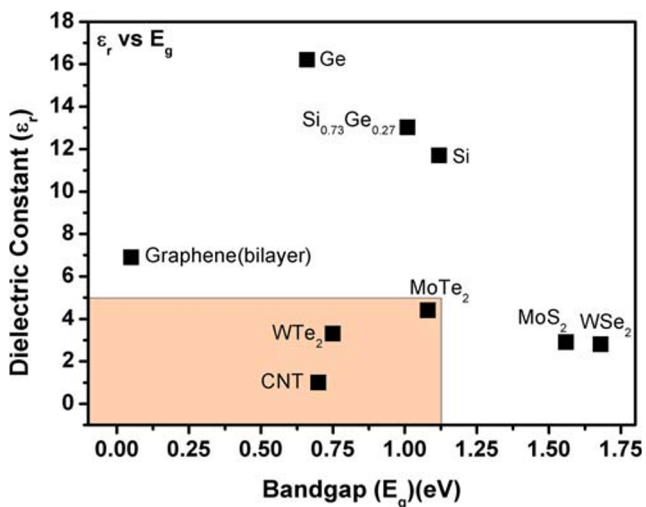
Fig. 4 Plot of dielectric constant versus band gap for various materials

Fig. 6 Plot of dielectric constant versus effective mass of electrons for various materials

4 Construction of the fundamental decision matrix

The value of band gap (E_g), dielectric constant (ε_r), and the effective mass of electrons $\left(m_l^*, m_t^*\right)$ can be easily found in the literature [3, 39, 41, 47–56] and are used verbatim. The electron effective mass of conductivity $\left(m_{cc}^*\right)$ and the on-state current to off-state current ratio, however, aren't explicitly provided, and have to be derived from the property tables. The electron effective mass of conductivity is calculated by finding the harmonic mean of the longitudinal and the transverse effective masses as has been shown by Barber [55]:

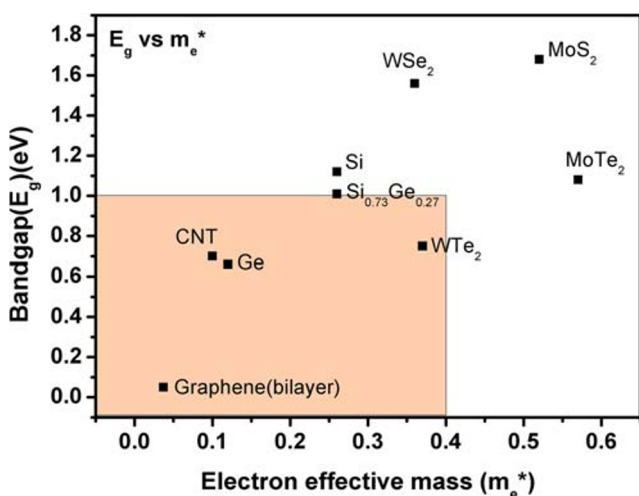$$m_e^* = m_{cc}^* = \frac{3}{\left(\dfrac{1}{m_l^*} + \dfrac{2}{m_t^*}\right)} \tag{16}$$

Table 1 displays the materials for which electron effective mass of conductivity is calculated in this manner.

The on-state current to the off-state current ratio is found by extrapolating the output and transfer characteristics to obtain appropriate readings. The on-state is defined as the point when V_{GS} and V_{DS} are both 0.5 V. The current flowing through the device at this point is the on-state current or I_{on}. The off-state is defined as the point when $V_{GS} = 0$ V, and the current through the device at this point is termed the off-state current (I_{off}). The ratio is defined as follows:

$$\frac{I_{on}}{I_{off}} = \frac{I_{DS}(V_{GS} = 0.5\ V, V_{DS} = 0.5\ V)}{I_{DS}(V_{GS} = 0\ V)} \tag{17}$$

Following the same train of thought as the one that was demonstrated in the Section 2 of this paper, and due to ITRS recommendations, it can be said that E_g, ε_r, m_e^* should have small values and are, therefore, treated as cost parameters. On the other hand, as recommended by the ITRS, and with due concern to the proper functioning of the device, on-state to off-state current ratio (I_{on}/I_{off}) needs to be high and is modeled as a profit parameter.

Table 2 shows the completed fundamental decision matrix.

Fig. 5 Plot of band gap versus effective mass of electrons for various materials

Table 3 Figure of merit values for materials shortlisted by Ashby methodology

Material	Figure of merit
CNT	1.8347×10^2
WTe$_2$	3.1015×10^1

Table 4   Weighted-normalised fundamental decision matrix

Material	$0.45E_g$	$0.35\varepsilon_r$	$0.1m_e^*$	$0.1\frac{I_{on}}{I_{off}}$
MoS$_2$	2.3687×10^{-1}	5.1418×10^{-2}	3.8029×10^{-2}	2.9851×10^{-7}
MoTe$_2$	1.5228×10^{-1}	5.6362×10^{-2}	5.9760×10^{-2}	2.2886×10^{-6}
WSe$_2$	2.1995×10^{-1}	3.5597×10^{-2}	3.9387×10^{-2}	4.5772×10^{-6}
WTe$_2$	1.0575×10^{-1}	3.6586×10^{-2}	4.4820×10^{-2}	1.2637×10^{-4}
CNT	9.8698×10^{-2}	9.8881×10^{-3}	1.3582×10^{-2}	9.9504×10^{-7}
Si$_{0.73}$Ge$_{0.27}$	1.4239×10^{-1}	2.5709×10^{-2}	1.7690×10^{-1}	9.9504×10^{-3}
Si	1.5792×10^{-1}	2.5709×10^{-2}	1.5891×10^{-1}	9.9504×10^{-2}
Ge	9.3199×10^{-2}	1.1866×10^{-2}	2.2003×10^{-1}	9.9504×10^{-7}

5 Results and Discussion

The different results of the material selection methods are presented here and discussed in detail.

5.1 Ashby Analysis

In this analysis, first, the Ashby plots are plotted. These plots are scatter plots that show multiple properties (2 or more) of the materials in consideration in the same plot [34]. These plots then have the constraints applied to them which yield a possible set of materials. These materials are then ranked using the FOM.

Figure 4 depicts the plot between band gap and dielectric constant for all the low dimensional materials. As discussed earlier, E$_g$ has to be less than 1.12 eV and ε_r lesser than 5. This leads to the discarding of Si, Ge, Si$_{0.73}$Ge$_{0.27}$, Graphene, MoS$_2$ and WSe$_2$ as suitable materials. The materials that satisfy the conditions are shaded in the figure.

Figure 5 depicts the plot between band gap and effective mass for all the low dimensional materials. As discussed earlier, E_g has to be less than 1.12 eV and m_e^* less than 0.4m_0, where m$_0$ is the rest mast of a free electron. This again leads to filtering of materials like Si, WSe$_2$, MoS$_2$, WTe$_2$ that violate the applied constraints. Again, the appropriate materials are in the shaded region of the figure.

Table 5   TOPSIS NIS, PIS and rank

Material	S$^-$	S$^+$	RC*	Rank
MoS$_2$	1.820×10^{-1}	1.812×10^{-1}	5.010×10^{-1}	5
MoTe$_2$	1.812×10^{-1}	1.329×10^{-1}	5.767×10^{-1}	3
WSe$_2$	1.826×10^{-1}	1.652×10^{-1}	5.250×10^{-1}	4
WTe$_2$	2.197×10^{-1}	1.082×10^{-1}	6.699×10^{-1}	2
CNT	2.527×10^{-1}	9.965×10^{-2}	7.172×10^{-1}	1
Si$_{0.73}$Ge$_{0.27}$	1.087×10^{-1}	1.932×10^{-1}	3.600×10^{-1}	8
Si	1.442×10^{-1}	1.598×10^{-1}	4.743×10^{-1}	6
Ge	1.504×10^{-1}	2.291×10^{-1}	3.962×10^{-1}	7

Figure 6 depicts the plot between effective mass and dielectric constant for all the low dimensional materials. As discussed earlier, m_e^* has to be lesser than 0.4m_0, where m_0 is the rest mast of a free electron and ε_r lesser than 5. After rejecting the materials like Graphene, Ge, Si, Si$_{0.73}$Ge$_{0.27}$, MoS$_2$, MoTe$_2$ that don't fit the constraint, the appropriate materials are selected, and are shown in the shaded region of the figure.

The materials that satisfy all the constraints are: CNT and WTe$_2$. These materials are then ranked according to the FOM function and it becomes evident that CNT is the best material, followed by WTe$_2$. The FOM are shown in Table 3.

5.2 TOPSIS Analysis

It has been noticed that Graphene has an extremely low on-state to off-state current ratio, which is shown to be less than 10 [52], and it also possesses a miniscule band gap that favours leakage current in the off-state. These reasons make it unfit to be considered as an ideal candidate and is excluded from all discussions henceforth.

For TOPSIS and VIKOR, it is necessary to figure out a weight matrix with germane justifications. As discussed in Section 2 of this paper, the band gap is a major concern for a TFET as it is one of the most crucial parameters, and is accordingly awarded the maximum weight. This is followed by the material dielectric constant, which is deemed a determining factor in permitting the technology to be scalable. These two are followed by effective mass of electrons and the on-state to off-state current ratio. The weights allotted need to follow criterion of their being normalised to one, i.e., $\sum_{j=1}^{n} w_j = 1$. Therefore, the weight matrix for normalisation is chosen as W = [0.45, 0.35, 0.1, 0.1]. Table 4 depicts the weighted-normalised matrix as was discussed in Section 3.2.

From the weighted-normalised matrix one can find the PIS (S^+) and the NIS (S^-).

$$S^+ = \{0.0932, 0.0099, 0.0136, 0.0995\}$$
$$S^- = \{0.2369, 0.0564, 0.2200, 0.0000\}$$

Table 6 VIKOR GU, IR, QI and ranks (*Corr. Rank = Corresponding Rank*)

Material	GU_i	Corr. rank	IR_i	Corr. rank	QI_i	Corr. rank
MoS$_2$	6.808×10^{-1}	8	4.500×10^{-1}	8	1.0000×10^{0}	8
MoTe$_2$	4.633×10^{-1}	4	1.850×10^{-1}	3	4.2867×10^{-1}	3
WSe$_2$	5.960×10^{-1}	7	3.970×10^{-1}	7	8.4915×10^{-1}	7
WTe$_2$	2.495×10^{-1}	2	9.987×10^{-2}	1	1.1743×10^{-1}	2
CNT	1.172×10^{-1}	1	9.999×10^{-2}	2	1.7994×10^{-4}	1
Si$_{0.73}$Ge$_{0.27}$	5.550×10^{-1}	6	2.768×10^{-1}	5	6.4116×10^{-1}	5
Si	4.831×10^{-1}	5	2.463×10^{-1}	4	5.3384×10^{-1}	4
Ge	4.542×10^{-1}	3	3.500×10^{-1}	6	6.5620×10^{-1}	6

Table 5 gives the distance from the PIS and NIS, relative closeness (RC*) to the ideal solution and the corresponding ranks.

Therefore, it is seen that CNT is the best material, followed by WTe$_2$ and MoTe$_2$.

5.3 VIKOR analysis

The weight matrix W required for the calculations is chosen to be the same as the one used for TOPSIS, i.e., W = [0.45, 0.35, 0.1, 0.1]. As was discussed in Section 3.3, the maximum and minimum values of group utility (GU) and individual regret (IR) of each opponent are calculated.

$$GU^- = \max(GU_i) = 0.6808$$
$$GU^* = \min(GU_i) = 0.1172$$
$$IR^- = \max(IR_i) = 0.4500 IR^*$$
$$\quad = \min(IR_i) = 0.0999$$

Using these values, the quality index (QI) is found and the ranks have been allotted as is depicted in Table 6.

$$QI\left(M^{''}\right) - QI\left(M^{'}\right) = QI(WTe_2) - QI(CNT) = 0.1172 \quad (17)$$

$$DQ = \frac{1}{8-1} = 0.1428 \quad (18)$$

$$QI\left(M^{''}\right) - QI\left(M^{'}\right) = QI(MoTe_2) - QI(CNT) = 0.4285 \quad (19)$$

Since $QI(M^{''}) - QI(M^{'}) \ngtr DQ$, we have a violation of the rule of accepted advantage. Therefore, a set of alternatives is offered as the compromise solution. We observe that $QI(M^{(u)})$

Table 7 Data to check validity of results

Performance Parameter	CNT [41, 57, 58]	WTe$_2$ [39]	MoTe$_2$ [39]
I_{on} ($\mu A/\mu m$)	2000	127	2.3
I_{on}/I_{off}	10^3 - 10^{10}	1.27×10^5	2.3×10^3
SS (mV/dec)	19.6	~19	~20

$- QI(M^{'}) < DQ$ till u = 2, which means that both $M^{'}$ and $M^{''}$ are the best alternatives.

Therefore, it can be concluded that CNT and WTe$_2$ are the best choices.

As a result of all three analyses, it can be said that CNT is the best material to choose as a TFET substrate, followed by WTe$_2$. To further build on this, MoTe$_2$ can be another suitable substrate choice for future high performance, high on-current TFETs.

5.4 Validation

The findings of the proposed work have been compared with other researchers work [39, 41, 57, 58] to verify their aptness and as a result, validate them. Table 7 lists I_{on}, I_{on}/I_{off}, SS and serves to perform a comparative analysis of TFET employing different low dimensional material substrates, namely, CNT, WTe$_2$, and MoTe$_2$. CNT displays a clear dominance in terms of the I_{on} and I_{on}/I_{off}. It also has comparable values of SS as compared to WTe$_2$. The closed match between the outcome of this work and the work of other researchers shows the validity of the proposed analysis for a high on-current TFET transistor. In order to further improve on the performance indices of the device, various strategies like optimised material synthesis procedures and differential doping of the device should be studied.

6 Conclusion

This paper highlighted the importance of low dimensional materials for achieving high on-current in a TFET transistor. The values of all the intrinsic material indices are taken from literature while the extrinsic parameters are calculated by extrapolating from graphical trends. Three different material selection approaches like Ashby, TOPSIS and VIKOR are employed to determine the best substrate. All three analyses demonstrate solidarity in their result and single out CNT as the candidate with the most potential for TFETs.

References

1. Yong-Bin K (2010) Challenges for Nanoscale MOSFETs and emerging Nanoelectronics. Trans Electr Electron Mater 11:93. https://doi.org/10.4313/TEEM.2009.10.2.021

2. Chopra S, Subramaniam S (2015) A review on challenges for MOSFET scaling. Int J Innov Sci Eng Technol 2:1055–1057

3. Taur Y, Ning TH (2009) Fundamentals of modern VLSI Devices

4. Yau LD (1974) A simple theory to predict the threshold voltage of short-channel IGFET's. Solid State Electron 17:1059–1063

5. Model TV, Devices LC (2005) Threshold voltage model. in: mosfet modeling & BSIM3 user's guide. pp 65–103

6. Tamak P, Mehra R (2017) Review on tunnel field effect transistors (TFET). Int Res J Eng Technol 4:1195–1200

7. Esseni D, Pala M, Palestri P et al (2017). A review of selected topics in physics based modeling for tunnel field-effect transistors Semicond Sci Technol:32. https://doi.org/10.1088/1361-6641/aa6fca

8. Lu H, Seabaugh A (2014) Tunnel field-effect transistors: state-of-the-art. IEEE J Electron Devices Soc 2:44–49. https://doi.org/10.1109/JEDS.2014.2326622

9. Madan J, Chaujar R (2016) Gate drain-overlapped-asymmetric gate dielectric-GAA-TFET: a solution for suppressed ambipolarity and enhanced ON state behavior. Appl Phys A Mater Sci Process 122:1–9. https://doi.org/10.1007/s00339-016-0510-0

10. Boucart K, Ionescu AM (2007) Double-gate tunnel FET with high-κ gate dielectric. IEEE Trans Electron Devices 54:1725–1733. https://doi.org/10.1109/TED.2007.899389

11. Madan J, Gupta RS, Chaujar R (2017) Performance investigation of heterogeneous gate dielectric-gate metal engineered–gate all around-tunnel FET for RF applications. Microsyst Technol 23:4081–4090. https://doi.org/10.1007/s00542-016-3143-5

12. Verhulst AS, Vandenberghe WG, Maex K, Groeseneken G (2007) Tunnel field-effect transistor without gate-drain overlap. Appl Phys Lett 91:1–4. https://doi.org/10.1063/1.2757593

13. Mallik A, Chattopadhyay A, Guin S, Karmakar A (2013) Impact of a spacer-drain overlap on the characteristics of a silicon tunnel field-effect transistor based on vertical tunneling. IEEE Trans Electron Devices 60:935–943. https://doi.org/10.1109/TED.2013.2237776

14. Naderi A, Keshavarzi P (2012) The effects of source/drain and gate overlap on the performance of carbon nanotube field effect transistors. Superlattice Microst 52:962–976. https://doi.org/10.1016/j.spmi.2012.07.016

15. Lee HK, Choi WY (2013) Linearity of hetero-gate-dielectric tunneling field-effect transistors. J Semicond Technol Sci 13:551–555. https://doi.org/10.5573/JSTS.2013.13.6.551

16. Kumar D, Dasgupta S, Ts JDS, et al (2017) With high on current and reduced turn on voltage

17. Gandhi R, Chen Z, Singh N et al (2011) Vertical Si-nanowire n-type tunneling FETs with low subthreshold swing (≤50 mV/decade) at room temperature. IEEE Electron Device Lett 32:437–439. https://doi.org/10.1109/LED.2011.2106757

18. Vishnoi R, Kumar MJ (2014) Compact analytical drain current model of gate-all-around nanowire tunneling FET. IEEE Trans Electron Devices 61:2599–2603. https://doi.org/10.1109/TED.2014.2322762

19. Arun Samuel TS, Arumugam N, Chandra ST (2017) Analytical approach and simulation of GaN single gate TFET and gate all around TFET. Trans Electr Eng Electron Commun 15:1–7

20. Beneventi GB, Gnani E, Gnudi A et al (2014) Dual-metal-gate InAs tunnel FET with enhanced turn-on steepness and high on-current. IEEE Trans Electron Devices 61:776–784. https://doi.org/10.1109/TED.2014.2298212

21. Kao KH, Verhulst AS, Vandenberghe WG et al (2012) Optimization of gate-on-source-only tunnel FETs with counter-doped pockets. IEEE Trans Electron Devices 59:2070–2077. https://doi.org/10.1109/TED.2012.2200489

22. Mitra SK, Bhowmick B (2019) An analytical drain current Model of gate-on-source/channel SOI-TFET. Silicon. https://doi.org/10.1007/s12633-019-0090-7

23. Yang Z (2016) Tunnel field-effect transistor with an L-shaped gate. IEEE Electron Device Lett 37:839–842. https://doi.org/10.1109/LED.2016.2574821

24. Convertino C, Zota CB, Schmid H et al (2018) III-V heterostructure tunnel field-effect transistor. J Phys Condens Matter 30. https://doi.org/10.1088/1361-648X/aac5b4

25. Kim G, Lee J, Kim JH, Kim S (2019) High on-current Ge-channel heterojunction tunnel field-effect transistor using direct band-to-band tunneling. Micromachines 10. https://doi.org/10.3390/mi10020077

26. Singh A, Khosla M, Raj B (2017) Design and analysis of electrostatic doped Schottky barrier CNTFET based low power SRAM. AEU - Int J Electron Commun 80:67–72. https://doi.org/10.1016/j.aeue.2017.06.030

27. Lam KT, Cao X, Guo J (2013) Device performance of heterojunction tunneling field-effect transistors based on transition metal dichalcogenide monolayer. IEEE Electron Device Lett 34:1331–1333. https://doi.org/10.1109/LED.2013.2277918

28. Balaji Y, Smets Q, Lockhart De La Rosa CJ et al (2018) Tunneling transistors based on MoS2/MoTe2Van der Waals Heterostructures. IEEE J Electron Devices Soc 6:1018–1055. https://doi.org/10.1109/JEDS.2018.2815781

29. Jena D (2013) Tunneling transistors based on Graphene and 2-D crystals. Proc IEEE 101:1585–1602. https://doi.org/10.1109/JPROC.2010.2070470

30. Gupta N, Haldiya V (2018) High-k gate dielectric selection for germanium based CMOS devices. Int J Nanoelectron Mater 11:119–126

31. Kandpal K, Gupta N (2016) Investigations on high-κ dielectrics for low threshold voltage and low leakage zinc oxide thin-film transistor, using material selection methodologies. J Mater Sci Mater Electron 27:5972–5981. https://doi.org/10.1007/s10854-016-4519-0

32. Deshmukh D, Angira M (2019) Investigation on switching structure material selection for RF-MEMS shunt capacitive switches using Ashby, TOPSIS and VIKOR. Trans Electr Electron Mater 20:181–188. https://doi.org/10.1007/s42341-018-00094-3

33. Ashby MF (2000) Multi-objective optimization in material design and selection. Acta Mater 48:359–369. https://doi.org/10.1016/S1359-6454(99)00304-3

34. Ashby M (2010) Materials selection in mechanical design: fourth edition

35. Hwang CL, Masud ASM (1979) Multiple objective decision making - methods and applications. Lect Notes Econ Math Syst 1:358. https://doi.org/10.1007/978-3-642-45511-7

36. Opricovic S, Tzeng GH (2004) Compromise solution by MCDM methods: a comparative analysis of VIKOR and TOPSIS. Eur J Oper Res 156:445–455. https://doi.org/10.1016/S0377-2217(03)00020-1

37. Lv Y, Qin W, Wang C et al (2019) Recent advances in low-dimensional Heterojunction-based tunnel field effect transistors. Adv Electron Mater 5:1–15. https://doi.org/10.1002/aelm.201800569

38. Roy T, Tosun M, Kang JS et al (2014) Field-effect transistors built from all two-dimensional material components. ACS Nano 8:6259–6264. https://doi.org/10.1021/nn501723y

39. Ilatikhameneh H, Tan Y, Novakovic B et al (2015) Tunnel field-effect transistors in 2-D transition metal Dichalcogenide materials. IEEE J Explor Solid-State Comput Devices Circuits 1:12–18. https://doi.org/10.1109/JXCDC.2015.2423096

40. Strojnik M, Kovic A, Mrzel A, et al (2014) MoS 2 nanotube field effect transistors. AIP Adv 4:0–5. https://doi.org/10.1063/1.4894440

41. Appenzeller J, Lin YM, Knoch J et al (2005) Comparing carbon nanotube transistors - the ideal choice: a novel tunneling device design. IEEE Trans Electron Devices 52:2568–2576. https://doi.org/10.1109/TED.2005.859654

42. Jiang XW, Li SS (2014) Performance limits of tunnel transistors based on mono-layer transition-metal dichalcogenides. Appl Phys Lett 104:1–5. https://doi.org/10.1063/1.4878515

43. Jahan A, Ismail MY, Sapuan SM, Mustapha F (2010) Material screening and choosing methods - a review. Mater Des 31:696–705. https://doi.org/10.1016/j.matdes.2009.08.013

44. Liao TW (2015) Two interval type 2 fuzzy TOPSIS material selection methods. Mater Des 88:1088–1099. https://doi.org/10.1016/j.matdes.2015.09.113

45. Mousavi-Nasab SH, Sotoudeh-Anvari A (2017) A comprehensive MCDM-based approach using TOPSIS, COPRAS and DEA as an auxiliary tool for material selection problems. Mater Des 121:237–253. https://doi.org/10.1016/j.matdes.2017.02.041

46. Opricovic S (1998) Multicriteria optimization of civil engineering systems

47. Léonard F, Tersoff J (2003) Dielectric response of semiconducting carbon nanotubes. Appl Phys Lett 81:4835–4837. https://doi.org/10.1063/1.1530373

48. Trivedi AR, Amir MF, Mukhopadhyay S (2014) Ultra-low power electronics with Si/Ge tunnel FET. 1–6. https://doi.org/10.7873/date.2014.244

49. Samuel TSA, Balamurugan NB (2014) Analytical modeling and simulation of germanium single gate silicon on insulator TFET. J Semicond 35. https://doi.org/10.1088/1674-4926/35/3/034002

50. Bessler R, Duerig U, Koren E (2019) The dielectric constant of a bilayer graphene interface. Nanoscale Adv 1:1702–1706. https://doi.org/10.1039/c8na00350e

51. Zhang Y, Tang TT, Girit C et al (2009) Direct observation of a widely tunable bandgap in bilayer graphene. Nature 459:820–823. https://doi.org/10.1038/nature08105

52. Fiori G, Iannaccone G (2009). On the possibility of tunable-gap bilayer graphene FET 30:261–264

53. Haddara YM, Ashburn P, Bagnall DM (2017) Silicon-germanium: properties, growth and applications. In: Kasap S, Capper P (eds) Springer handbook of electronic and photonic materials. Springer International Publishing, Cham, p 1

54. Huang C-TT (2015) Electrical and material properties of strained silicon/relaxed silicon germanium Heterostructures for single-Electron quantum dot applications. 1–127

55. Barber HD (1967) Effective mass and intrinsic concentration in silicon. Solid State Electron 10:1039–1051. https://doi.org/10.1016/0038-1101(67)90122-0

56. Sze SM, Ng KK (2006) Appendix F properties of important semi-conductors. In: physics of semiconductor Devices. John Wiley & Sons, Ltd, p 789

57. Zhou HL, Jiang J, Zhang MX, Fang L (2010) Opitimization of tunneling carbon nanotube-FETs based on stair-case doping strategy. Sci China Inf Sci 53:2696–2704. https://doi.org/10.1007/s11432-010-4102-x

58. Javey A, Tu R, Farmer DB et al (2005) High performance n-type carbon nanotube field-effect transistors with chemically doped contacts. Nano Lett 5:345–348. https://doi.org/10.1021/nl047931j